ATL-PHYS-2000-003
11/01/2000

Prospect for QCD Jet Studies in ATLAS

Hasko Stenzel[a] and Stefan Tapprogge[b]

a) MPI Munich
b) CERN - EP Division

Abstract

The understanding of the properties of QCD di-jet and multijet events is crucial for most of the searches to be carried out at LHC. But the study of jet production is also a stringent test of perturbative QCD in an energy regime never probed so far. In addition, measurements of the triple differential cross section can be used to constrain parton distribution functions. In this note a study of jet production features in terms of jet transverse momenta and di-jet invariant masses is performed, leading to an estimation of the kinematically explorable region and of present theoretical uncertainties.

1 Introduction

The understanding of the properties of QCD di-jet and multijet events is crucial for most of the searches to be carried out at LHC. But the study of jet production is also a stringent test of perturbative QCD in an energy regime never probed so far. In addition, measurements of the triple differential cross section can be used to constrain parton distribution functions. In this note a study of jet production features in terms of jet transverse momenta and di-jet invariant masses is performed, leading to an estimation of the kinematically explorable region and of present theoretical uncertainties.

The note is structured as follows: the next section describes the QCD calculations used, followed by a discussion of the ATLAS detector fast simulation. Next, the event selection and the corrections applied are described. Then the results are discussed for the inclusive jet cross-section and for di-jet production.

2 Leading order and next-to-leading order QCD generators

2.1 Leading order: PYTHIA

In PYTHIA [1] the hard scattering matrix elements are implemented in leading order (LO). The effects of higher orders are approximated (to leading log accuracy) by adding parton showers to the partons entering (initial state radiation) and being produced (final state radiation) in the hard scattering process. The hadronization of the multi parton system is performed using the Lund color string fragmentation model. In addition, PYTHIA can model the contribution from multiple parton interactions in the same event, i.e. the underlying event. For the studies presented in this note, the version 6.1 of PYTHIA has been used.

2.2 Next-to-leading order: JETRAD

The JETRAD program [2] includes the next-to-leading order (NLO) corrections to the LO hard scattering matrix element for the $2 \rightarrow 2$ process. Two contributions can be distinguished: the $2 \rightarrow 3$ real emission diagrams and the virtual loop corrections to the $2 \rightarrow 2$ diagrams. At NLO, there can be more than two partons in the final state and thus it is necessary to define jets also at the parton level (as two out of the three partons could be close and thus be not resolved into two jets). JETRAD generates weighted events (i.e. with two or three partons) at the parton level. No higher orders beyond NLO or hadronization are taken into account, as it is done in case of PYTHIA, were higher orders are approximated by the parton shower.

2.3 Definition of a pseudo K-factor

In general, the K-factor is defined as the ratio between the NLO and the LO cross-section:

$$K = \frac{\sigma_{NLO}}{\sigma_{LO}}. \tag{1}$$

The inclusion of higher order corrections often leads to an increase of the cross-section (i.e. a K-factor being larger than one) due to the appearance of new channels which are not allowed at leading order. It should be noted, however, that the K-factor can depend on kinematical variables, e.g. on the transverse energy.

For the study presented in this note, the following definition of a K-factor (called 'pseudo K-factor') is used:

$$K = \frac{\sigma_{NLO}(JETRAD)}{\sigma_{LO}(PYTHIA)}. \tag{2}$$

It is derived from the ratio of the NLO cross-section $\sigma_{NLO}(JETRAD)$ (as obtained from JETRAD) and the LO cross-section $\sigma_{LO}(PYTHIA)$, as obtained from PYTHIA.

3 Jet reconstruction in ATLAS and detector simulation

3.1 ATLFAST

ATLFAST [3] is a fast simulation of the response of the ATLAS detector. The main effects included are the smearing of the deposited energy and the effect of the magnetic field on the azimuthal position of particles.

The energies of all particles (except muons and neutrinos) are, after applying the effect of the solenoidal field of 2 T, summed into calorimeter cell matrices. The granularity of these cells (in terms of $\Delta\eta \times \Delta\phi$) is 0.1×0.1 for $|\eta| < 3$ and 0.2×0.2 for $3 < |\eta| < 5$. The energy in each cell is then smeared according to a function, which differs for low and high luminosity running. At low luminosity, the following jet energy resolutions are used, which have been obtained from full simulation of the detector response and have been validated by test beam measurements:

$$\frac{\sigma}{E} = \frac{0.5}{\sqrt{E}} \oplus 0.03 \qquad (|\eta| < 3) \tag{3}$$

and

$$\frac{\sigma}{E} = \frac{1.0}{\sqrt{E}} \oplus 0.07 \qquad (|\eta| > 3). \tag{4}$$

For the case of high luminosity, an additional smearing in transverse energy is done for each cell after the energy resolution induced smearing described above. The size of this pile-up contribution σ_{pileup} varies with the size R of the CONE: 7.5 GeV in E_T for $R = 0.4$ and 18 GeV in E_T for $R = 0.7$.

On these matrices a CONE jet algorithm is run, taking as initiators (seeds) all cells with a transverse energy of more than 1.5 GeV.

3.2 Optimization of cone size

The cone size of the jet algorithm was first optimized at parton level. Each event contains two jets (partons) as a result of the hard scattering process. All subsequent partons generated in the parton shower can unambiguously be assigned to a jet, using mother-daughter relationships. Adding the covariant four-momenta of all partons generated by the primary hard scattering products gives the 'true' parton jets. Parton jets were also

reconstructed using a cone algorithm and compared to true jets. The cone size is varied in order to maximize the fraction of transverse energy being contained inside the cone. At the same time the amount of energy entering in the reconstruction cone from other sources (underlying event and the other jet) increases with the cone size. An optimum cone size of $\Delta R = 1$ is found at parton level: this contains 92 % of the true jet transverse energy and 10 % of E_T contamination from other sources. Therefore with this cone size, out-of-cone losses are compensated by the energy flow of other sources.

In a second step the cone size is verified at hadron level. Reconstructed hadron jets can be matched to parton jets using a matching in the η-ϕ plane, where the assignment is based on minimising the distance:

$$\Delta R = \sqrt{(\eta_{parton} - \eta_{hadron})^2 + (\phi_{parton} - \phi_{hadron})^2}. \tag{5}$$

Here, η_{parton} (ϕ_{parton}) denotes the coordinates of the parton jets, η_{hadron} (ϕ_{hadron}) the ones of the hadron jet. At the hadron level, smaller cone sizes are preferred, because hadronization makes the jets broader and particle production occurs in the inter-jet region. Furthermore, larger cones enhance the contribution from detector electronic noise and pile-up noise. Therefore a cone size of $R = 0.8$ was used as a compromise to minimize out-of-cone and contamination correction on one side and to keep a good energy and angular resolution on the other side.

This study did not include the effect of pile-up events as well as from electronic noise and other effects on the absolute value of the energy associated with a jet at detector level. Only the effect on the energy resolution is taken into account, by adding an additional contribution to the energy smearing, as described above. The pile-up contribution to the absolute energy measurement at design luminosity is likely to give preference to a still smaller cone size [4].

3.3   Generated samples

For the following studies, four samples with different cut-offs on the minimal $\hat{p}_T$ of the hard scattering matrix element have been generated: $\hat{p}_T > 180, 500, 1000$ and 1380 GeV. These samples cover different kinematic regions, which do however overlap. For these overlap regions, the samples have been matched in luminosity. The last two values have been chosen such that the number of generated events corresponds to the expected statistics for an integrated luminosity of 30 fb^{-1} resp. 300 fb^{-1}. The sample with $\hat{p}_T > 1380$ GeV has been generated under high luminosity conditions, i.e. adding the additional term to smear the transverse energy, as described above. For these samples, tuned settings of PYTHIA have been used, as obtained from LEP and CLEO data [5]. As a parameterization of the proton structure function, the CTEQ2L [6] set has been used.

In the NLO calculation (JETRAD) the CTEQ4M [7] parton distribution set has been chosen.

4   Trigger, event selection and corrections

4.1   Cuts

For all the studies presented in this note, the single inclusive LVL1 jet trigger has been assumed. The threshold on the jet E_T is 180 GeV at low luminosity and 290 GeV at

high luminosity. The η range is restricted to $|\eta| < 3.2$. The efficiency of the trigger has been assumed to be 100 %, in reality it will be slightly lower (about 95 % w.r.t. an offline selection).

4.2   Correction for detector effects

The cross-section obtained is corrected (bin-by-bin) for detector effects by multiplying the content of each bin by a factor, which is determined from the ratio of the cross-section $\sigma_{hadron}(PYTHIA)$ from PYTHIA at the level of final state hadrons to the cross-section $\sigma_{detector}(PYTHIA + ATLFAST)$ from PYTHIA when the ATLFAST parameterization is applied to the final state hadrons.

Typical correction factors obtained as a function of the jet transverse energy are shown in Figure 1. The correction factor shows almost no dependence on the jet transverse energy
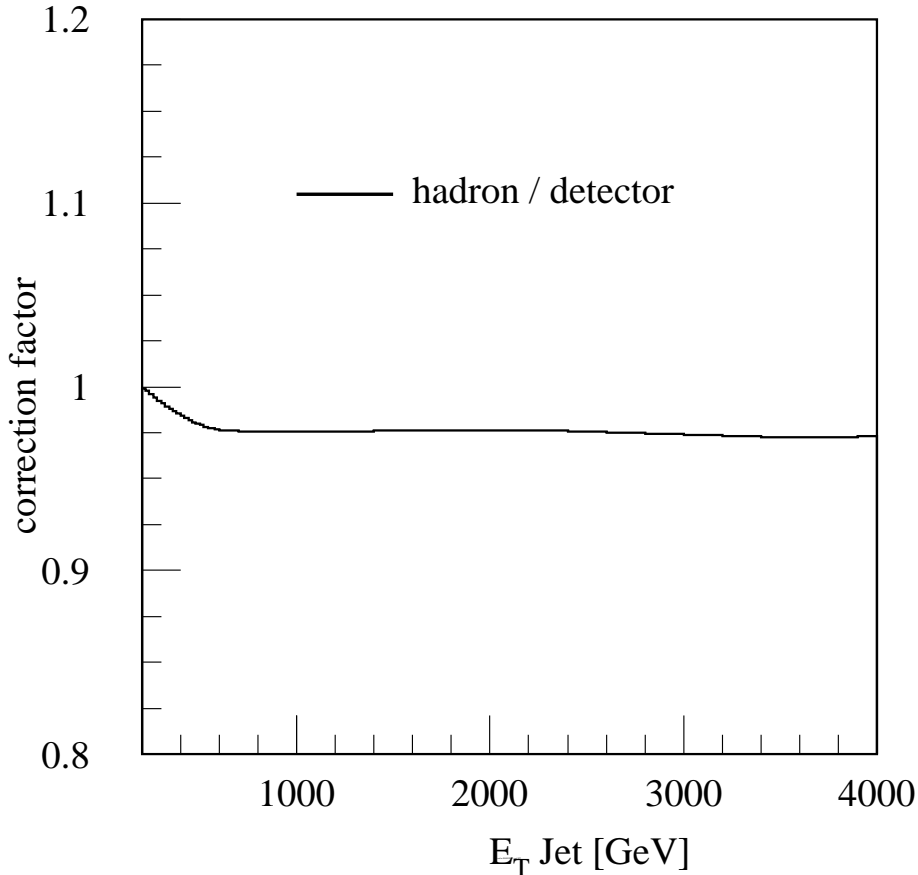

Figure 1: Detector correction factors for single inclusive jet production as a function of the minimal jet transverse energy E_T.

and is very close to 1 (about 0.975 for $E_T > 600$ GeV).

4.3   Correction for hadronization

Since the comparision of data and QCD calculation is performed at hadron level, theoretical parton level predictions must be corrected for hadronization effects. Here, the E_T-jet

cross-section predicted by JETRAD is corrected bin-by-bin for hadronization. This correction factor is once again determined using a bin-by-bin ratio of the hadron level cross-section $\sigma_{hadron}(PYTHIA)$ to the cross-section $\sigma_{parton}(PYTHIA)$ from PYTHIA at the parton level (i.e. after parton showers, but before hadronization). The correction factors for hadronization are shown in Figure 2. The correction for hadronization decreases sig-
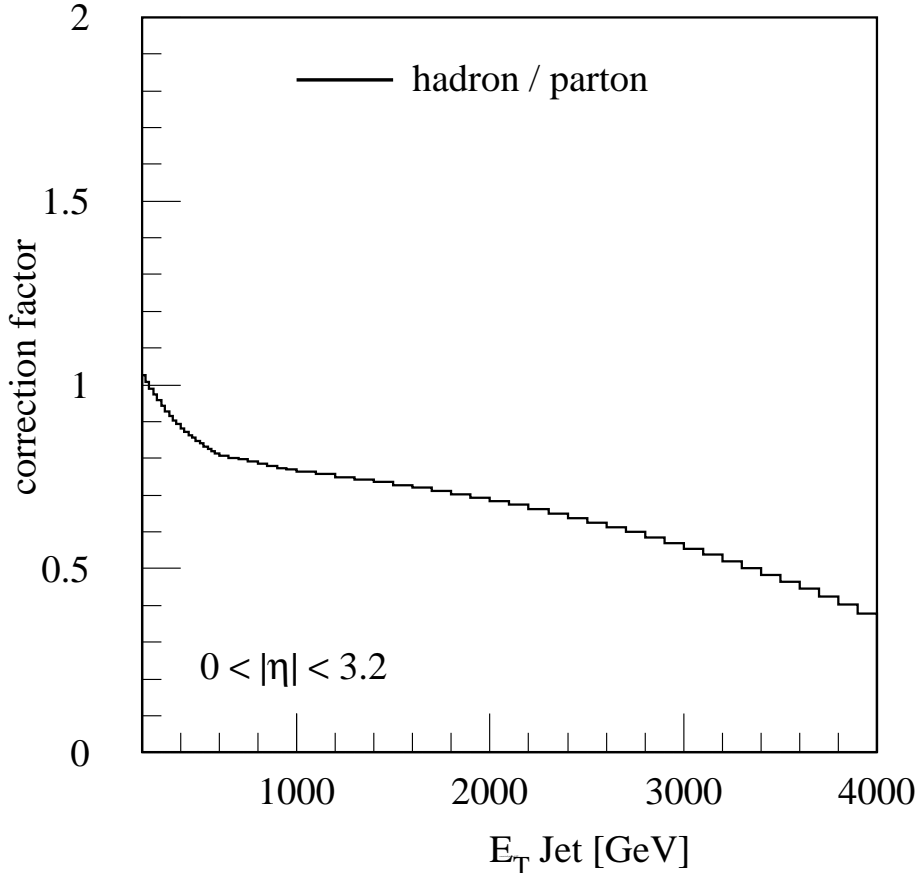

Figure 2: Hadronization correction factors for single inclusive jet production as a function of the minimal jet transverse energy E_T.

nificantly with increasing E_T of the jet and reaches a value of about 0.4 for $E_T = 4$ TeV. This behaviour of the correction function is not understood. The dependence of the jet shape on the jet energy leads to smaller jets at higher energies compared to the ones with smaller energy. This should however not influence the comparison between hadron level and parton level (where for the latter parton showers are included), as non-pertubative power corrections are expected to be suppressed like $1/Q$, where Q is the energy scale. More studies are needed in this area.

4.4   Higher order corrections

The hadron level cross-section obtained with PYTHIA and ATLFAST is first corrected for detector effects and then corrected for higher order QCD effects. This is done by

multiplying the cross-section by the pseudo K-factor defined above bin-by-bin. Pseudo K-factors for the single inclusive jet cross-section are shown in Figure 3. Theoretical systematic uncertainties of the pseudo K-factor are of the order of 10 %, as obtained from different values of the QCD parameter $\Lambda_{\overline{MS}}$ for CTEQ4M and from different sets of parton distribution functions (PDF's). The pseudo K factor increases with decreasing
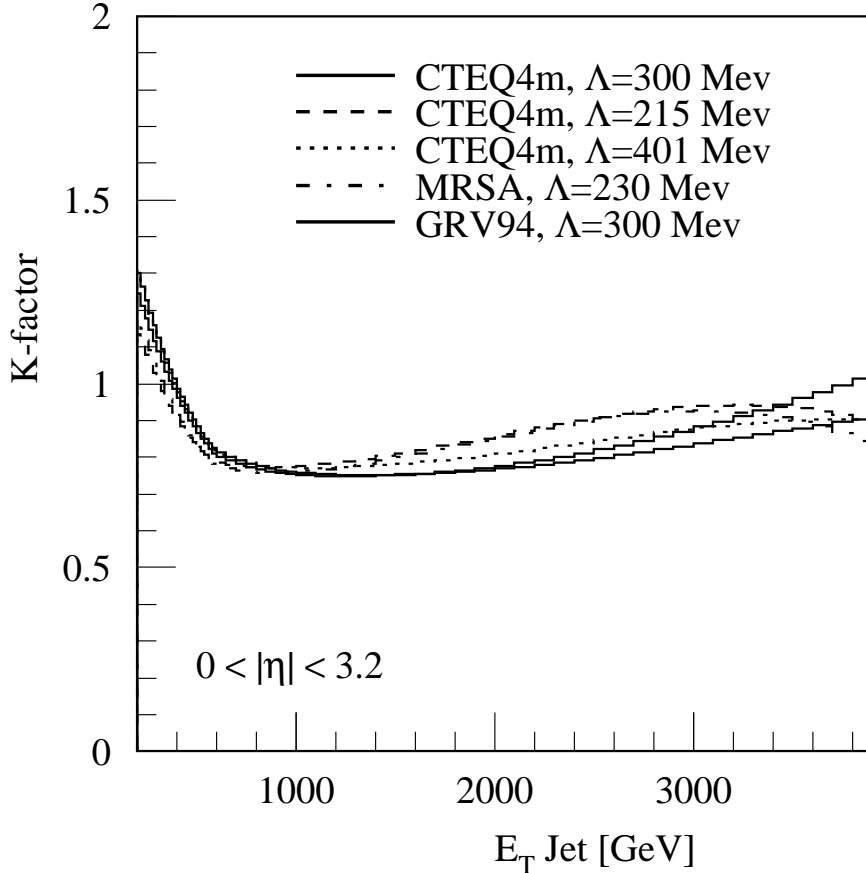

Figure 3: Pseudo K-factors for single inclusive jet production as a function of the minimal jet transverse energy E_T, for various PDF's.

E_T for jet transverse energies below 1 TeV and shows a slight increase with E_T for the region of $E_T > 1$ TeV. For jet transverse energies of $E_T > 400$ GeV, its value is smaller than 1.

4.5   Summary of corrections

The corrections described above can be summarized in the following two expressions, first for the cross-section resulting from unfolding of the (fast) detector simulation and second for the NLO calculation:

$$\sigma_{'data'} = \sigma_{ATLFAST} \cdot f_{detector} \cdot f_K \tag{6}$$

and

$$\sigma_{NLO} = \sigma_{JETRAD} \cdot f_{hadronization}, \tag{7}$$

6

where $f_{detector} = \sigma_{PYTHIA}/\sigma_{PYTHIA+ATLFAST}$, $f_K = K$ (the pseudo K-factor defined above) and $f_{hadronization} = \sigma_{hadron}(PYTHIA)/\sigma_{parton}(PYTHIA)$. All correction factors are applied on a bin-by-bin basis.

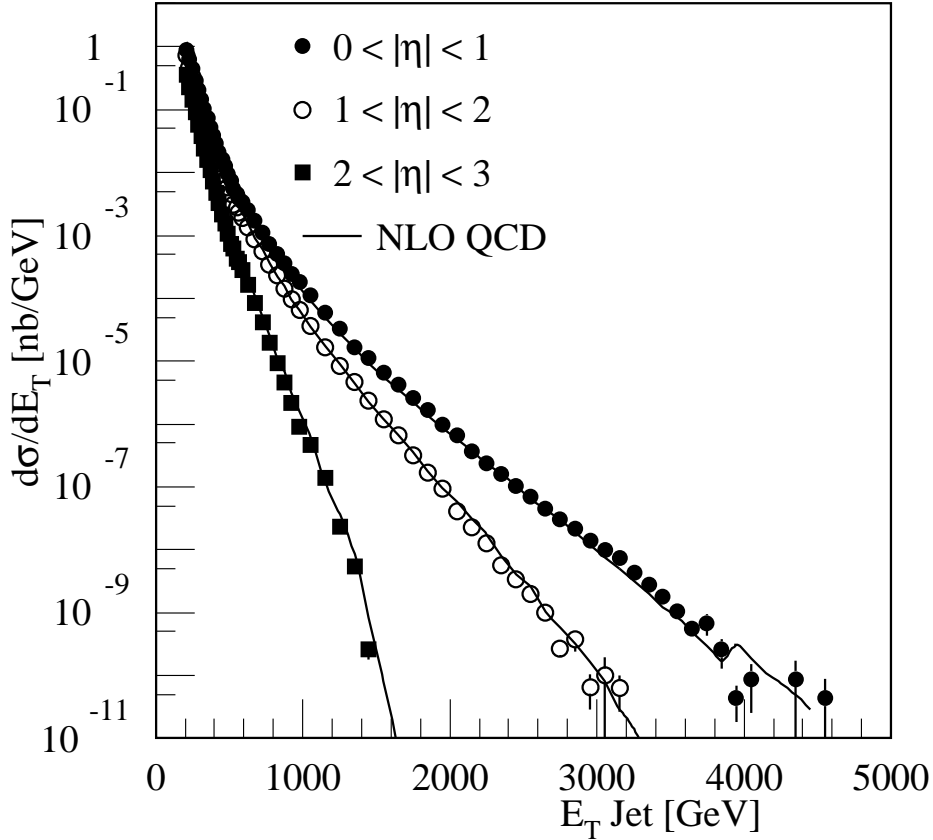# 5   Results

5.1   Inclusive single jet production

Figure 4: Cross-section for inclusive jet production as a function of the minimal jet transverse energy.

Figure 4 shows the inclusive jet cross-section as a function of the minimal jet transverse energy for three bins in pseudo-rapidity: $|\eta| < 1$, $1 < |\eta| < 2$ and $2 < |\eta| < 3$. The points correspond to the hadron level cross-section obtained from correcting the PYTHIA result passed through the ATLFAST detector simulation. The error bars correspond for large values of $E_T > 1$ TeV to the expected statistical uncertainty for an integrated luminosity of 300 fb^{-1}. For small values of E_T the statistical uncertainty will be completely negligible and systematic uncertainties like the knowledge of the energy scale will dominate. For values of $E_T > 1$ TeV, direct calibration of the jet energy scale using a physics process would be difficult and one has to rely on extrapolations from lower energies. The dominating overall uncertainty will be given by the knowledge of the absolute luminosity, which

is presently estimated to be measured to within 5 – 10 % and gives rise to a correlated error.

The cross-section falls steeply over 11 orders of magnitude, when starting at a minimal transverse energy of $E_T > 200$ GeV. For large values of E_T the cross-section of centrally produced jets is significantly higher than the one for jets produced in the forward direction. Also shown in the figure is the expected cross-section from the NLO calculation of JETRAD.

For an integrated luminosity of 30 fb^{-1}, about 40 events are expected with $E_T > 3$ TeV, 3000 events with $E_T > 2$ TeV and $4 \cdot 10^5$ events with $E_T > 1$ TeV.
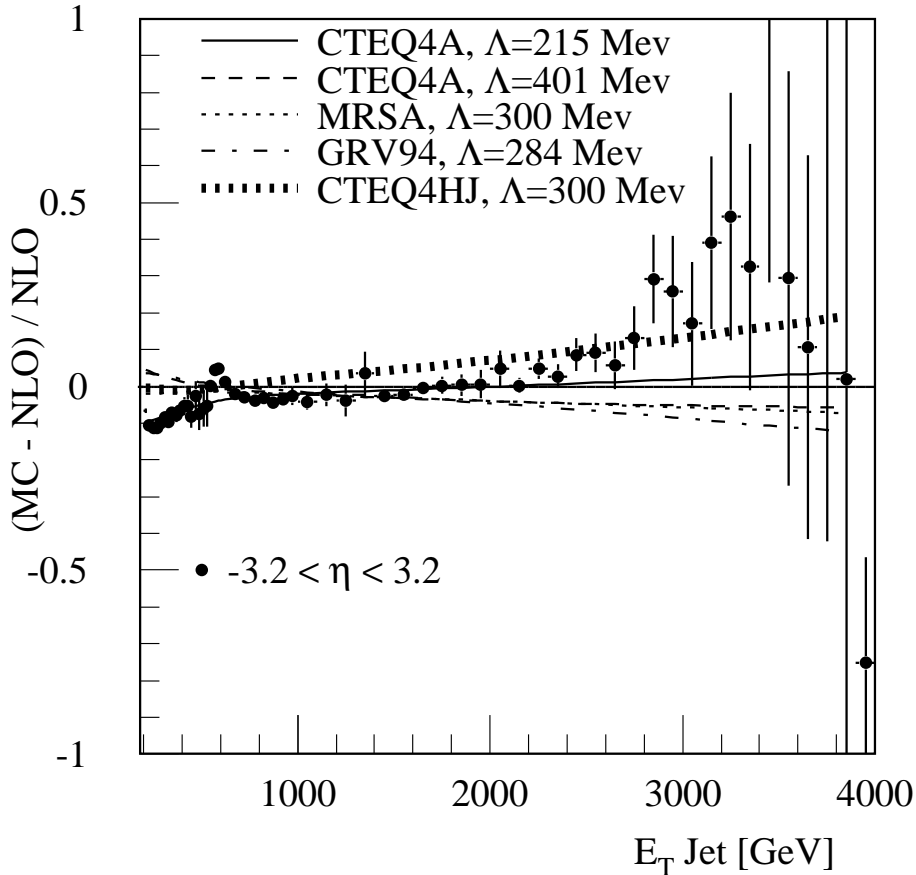

Figure 5: Relative difference of the PYTHIA cross-section for inclusive jet production to the one at NLO as a function of the minimal jet transverse energy.

To study the effect of varying the parton density parameterization and the strong coupling constant, in fig. 5 the relative difference of the cross-section obtained from PYTHIA ('MC') to the one of the JETRAD calculation ('NLO') is shown as a function of the minimal jet transverse energy for the full range in pseudo-rapidity ($|\eta| < 3.2$). Clearly visible in this figure are the remaining threshold effects from merging the four samples with different cuts on the minimal $\hat{p}_T$ for the hard scattering matrix element. The effect of choosing a different parton density is shown for the cases of MRSA [8], GRV94 [9] and CTEQ4HJ [7]. In these cases (also for the full range $|\eta| < 3.2$), the value of $\Lambda_{\overline{MS}}$ is fixed to 300 MeV (284 MeV for GRV94). The variation is most prominent for large values of E_T,

reaching up to about 15 %. The effect of different values of the strong coupling constant is depicted for the CTEQ4A [7] set, with $\Lambda_{\overline{\text{MS}}} = 215, 400$ MeV. The variation obtained is less than 5 %, even at large values of the jet E_T.
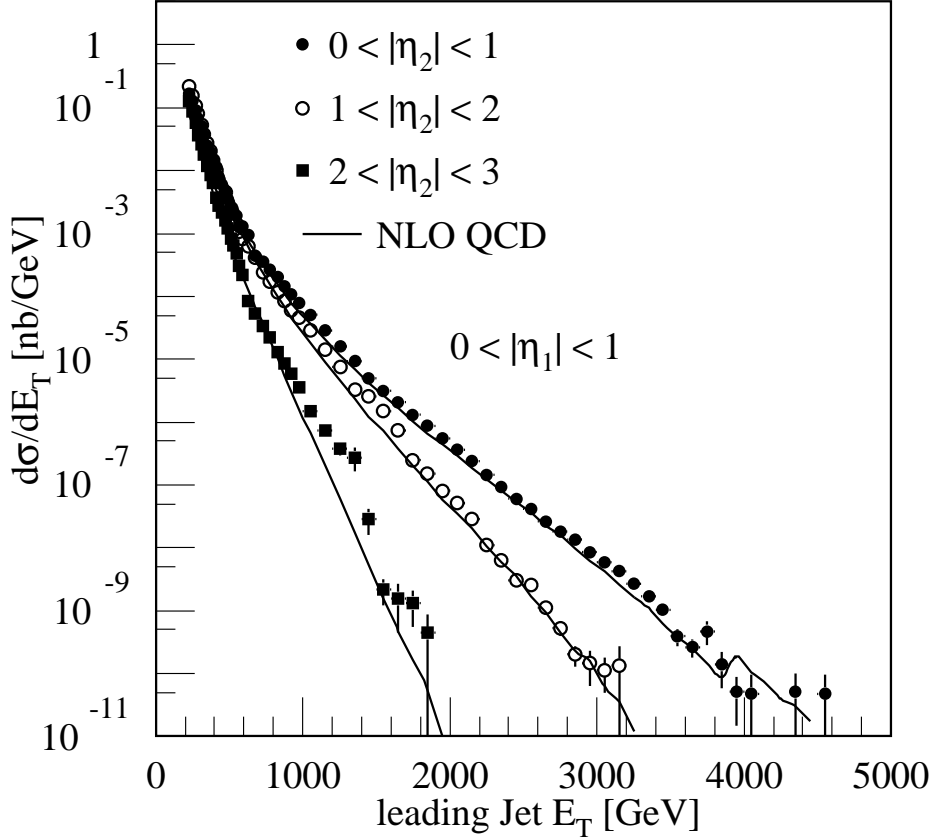
5.2 Di-jet production

Figure 6: Cross-section for di-jet production as a function of the minimal jet transverse energy.

Figure 6 shows the expected cross-section for di-jet production as a function of the E_T of the leading jet for different values of the pseudo-rapidity for the second leading jet: $|\eta_2| < 1$, $1 < |\eta_2| < 2$ and $2 < |\eta_2| < 3$. The leading jet is required to be at central rapidities ($|\eta_1| < 1$). Again, the error bars correspond to the expected statistical uncertainty for an integrated luminosity of 300 fb^{-1} at large E_T. Shown as well is the cross-section at NLO for the same cuts.

The measurement of di-jets and their properties (i.e. the transverse energy E_T of the leading jet and the pseudo-rapidities $\eta_{1,2}$ of the two jets) can be used to constrain the parton densities of the proton. From the measurement of E_T and of $\eta_{1,2}$, the parton momenta $x_{1,2}$ can be calculated (at leading order) using the following expression:

$$x_{1,2} = \frac{E_T}{\sqrt{s}} \left(e^{\pm \eta_1} + e^{\pm \eta_2} \right). \tag{8}$$
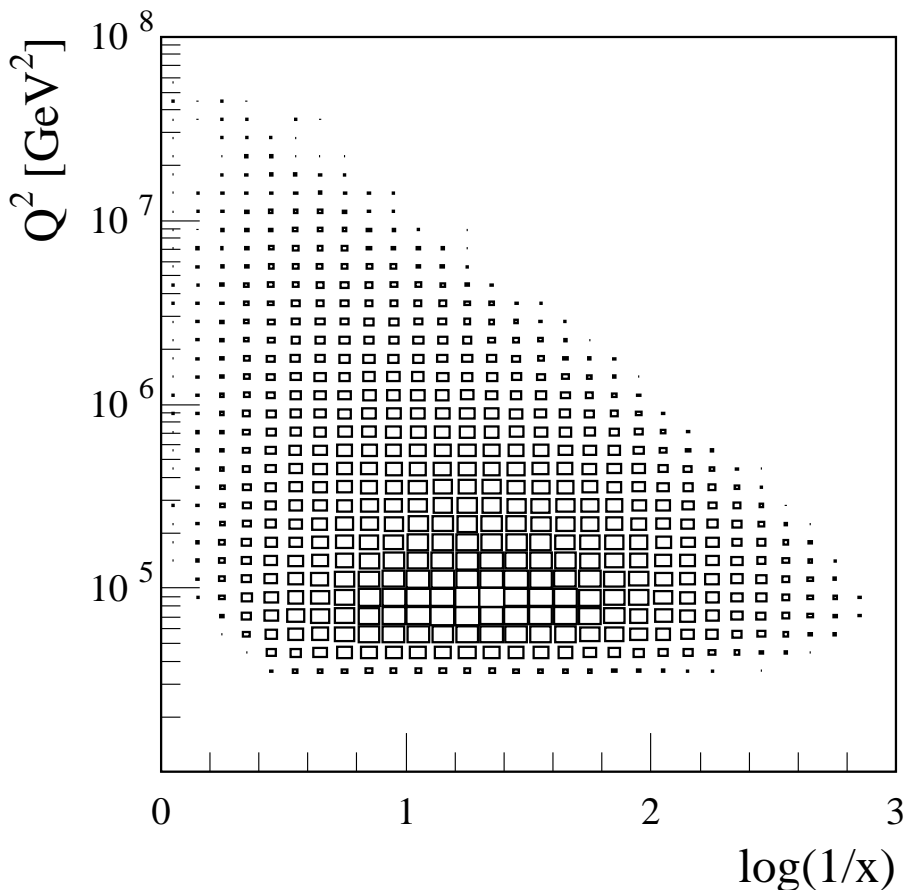
Figure 7: Reach in the $(1/x, Q^2)$ plane from di-jet production for $|\eta| < 3.2$ and $E_T > 180$ GeV.

The hard scattering scale Q^2 can be approximately obtained using the two variables E_T and $\eta^* = 0.5 \cdot |\eta_1 - \eta_2|$ with:

$$Q^2 \approx 2E_T^2 \cosh^2 \eta^* \left(1 - \tanh \eta^*\right). \tag{9}$$

In fig. 7 the reach in the kinematic plane $(1/x, Q^2)$ is shown for events with $E_T > 180$ GeV. Only those bins are displayed where the expected number of events is larger than 100 for an integrated luminosity of 300 fb^{-1}. The lower limit in Q^2 is due to the LVL1 trigger, which accepts only jets with $E_T > 180$ GeV (leading to $Q^2 > 3.2 \cdot 10^4$ GeV^2). The use of prescaled triggers with lower E_T thresholds will allow also the region of lower Q^2 values to be covered. For a lower limit of $Q^2 > 10^5$ GeV^2 (i.e. the kinematical limit of HERA), the range in x covered by the inclusive jet trigger corresponds to $2 \cdot 10^{-3} < x < 0.5$.

5.3   Di-jet invariant mass distribution

Figure 8 shows the cross-section for di-jet production as a function of the di-jet invariant mass for centrally produced di-jets ($|\eta_{jet}| < 1$). The cross-section extends over 11 orders of magnitude for invariant masses between 500 and 9000 GeV/c^2. For an integrated luminosity of 300 fb^{-1}, the available statistics should allow a measurement of masses up
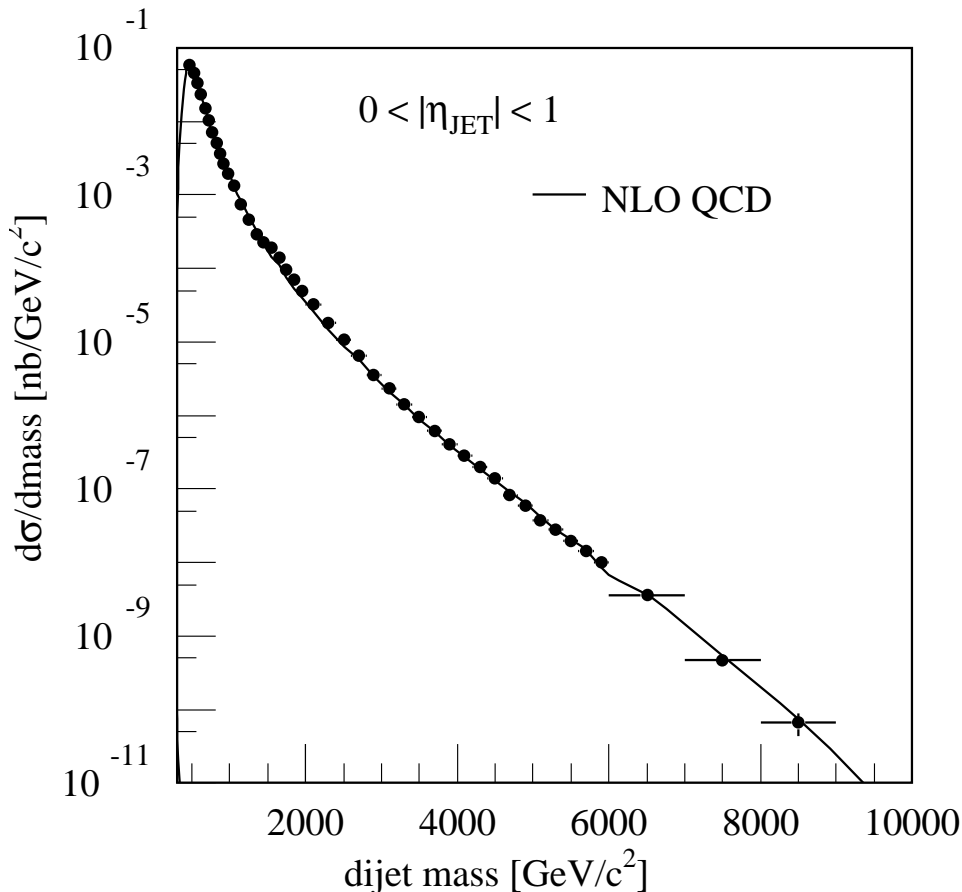
Figure 8: Cross-section for di-jet production as a function of the di-jet invariant mass.

to 10 TeV/c^2. Besides the corrected cross-section from PYTHIA plus ATLFAST, the prediction of JETRAD is shown.

In figure 9 the relative difference of the corrected PYTHIA plus ATLFAST cross-section to the JETRAD (NLO) cross-section is shown as a function of the di-jet invariant mass (for $|\eta| < 1$). Clearly visible are the residual threshold effects from the merging of the four samples of events generated with the different cuts on the minimal $\hat{p}_T$ for the hard scattering matrix element. Also shown is the ratio (again for $|\eta| < 1$) of the NLO calculation with different parton distribution function sets (MRSA, GRV94 and CTEQ4HJ) and with different values of the strong coupling constant (CTEQ4A, $\Lambda_{\overline{MS}} = 215, 401$ MeV) to the reference cross-section from JETRAD (CTEQ4M with $\Lambda_{\overline{MS}} = 300$ MeV).

6 Outlook

This note presented a first study on the inclusive single and di-jet production using the AT-LAS detector at the LHC. The potential of ATLAS to study high p_T scattering processes at the smallest distance scales with sufficient statistics has been shown, e.g. after three years of running at design luminosity about 400 events with jets of transverse energies above 3 TeV are expected. Not yet studied are the experimental systematic uncertainties which will in most cases be larger than the statistical error. Especially in the TeV region,
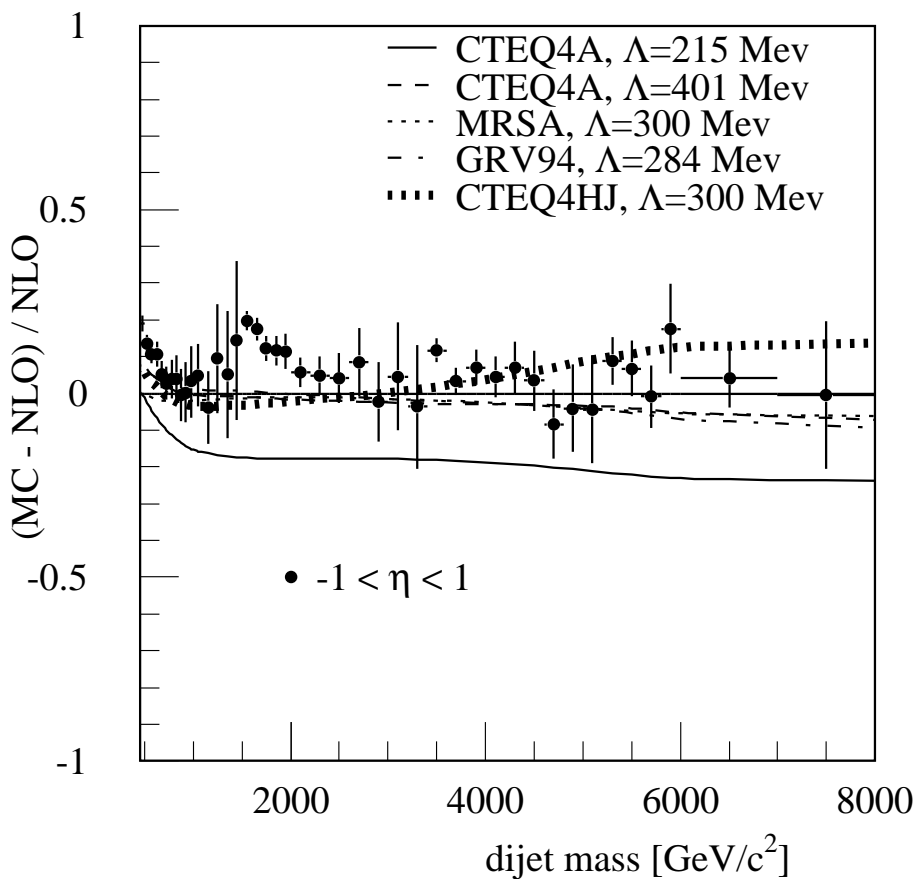
Figure 9: Relative difference of the PYTHIA cross-section for di-jet production to the one at NLO as a function of the di-jet invariant mass.

the knowledge of the jet energy scale will be one of the dominating uncertainties.

Further steps in the study of jet production could try to quantify the expected accuracy on the quark and the gluon densities, going together with the development of a strategy to extract parton densities from jet cross-section measurements. The aim should be to provide the expected accuracies as a function of the parton kinematical variables x and Q^2.

In this context, also the correlation between parton densities and the strong coupling constant should be addressed, and the possibilities of measuring α_s from hadron collider data should be evaluated. The triple differential di-jet cross-section could be used for a simultaneous extraction of the quark and gluon densities and the strong coupling constant. An alternative method for extracting the strong coupling constant could be provided by the ratio of the 3-jet cross-section to the 2-jet cross-section. This ratio should be much less dependent on the parton densities. A NLO calculation of the 3-jet cross-section has recently become available [10].

A further important topic related to jets is the study of the jet shape and fragmentation.

References

[1] T. Sjostrand, Comp. Phys. Comm. **82** (1994) 74.

[2] W.T. Giele et al., Nucl. Phys. **B403** (1993) 633.

[3] E. Richter-Was et al., ATLAS internal note ATL-PHYS-98-131 (1998).

[4] ATLAS Collaboration, Detector and Physics Performance Technical Design Report, CERN/LHCC 99-14/15 (1999).

[5] R. Barate et al., ALEPH Collaboration, Phys. Rep. **294** (1998) 1.

[6] Wu-Ki Tung, 'Perspectives on Global QCD Analyses', in Proceedings of the International Workshop on Deep Inelastic Scattering and Related Subjects, Eilat, Israel (1994), ed. A. Levy, World Scientific Publishing Co., Singapore

[7] H.L. Lai et al., Phys. Rev. **D55** (1997) 1280.

[8] A.D. Martin et al., Phys. Rev. **D50** (1994) 6734

[9] M. Gluck et al., Z. Phys. **C67** (1995) 433.

[10] W.B. Kilmore and W.T. Giele, preprint hep-ph **9903361** (1999).